Supporting Online Material

Structure of the human kappa opioid receptor in complex with JDTic

Huixian Wu[1], Daniel Wacker[1], Vsevolod Katritch[1], Mauro Mileni[1], Gye Won Han[1], Eyal Vardy[2], Wei Liu[1], Aaron A. Thompson[1], Xi-Ping Huang[2], F. Ivy Carroll[3], S. Wayne Mascarella[3] Richard B. Westkaemper[4], Philip D. Mosier[4], Bryan L. Roth[2], Vadim Cherezov,[1] Raymond C. Stevens[1*]

[1]Department of Molecular Biology, The Scripps Research Institute, 10550 North Torrey Pines Road, La Jolla, CA 92037, USA

[2]National Institute of Mental Health Psychoactive Drug Screening Program, Department of Pharmacology and Division of Chemical Biology and Medicinal Chemistry, University of North Carolina Chapel Hill Medical School, 4072 Genetic Medicine Building, Chapel Hill, NC 27514, USA

[3]Center for Organic and Medicinal Chemistry, Research Triangle Institute, P.O. Box 12194, Research Triangle Park, NC 27709, USA

[4]Department of Medicinal Chemistry, Virginia Commonwealth University, 800 E. Leigh Street, Richmond, VA 23298, USA

*To whom correspondence should be addressed: stevens@scripps.edu

Supplementary Tables:

Supplementary Table 1. Data collection and refinement statistics. Highest resolution shell is shown in parentheses.

Structure	hKOR	
Data collection		
Space group	$P2_12_12_1$	
Cell dimensions a, b, c (Å)	54.90, 147.30, 205.29	
Number of reflections measured	154,545	
Number of unique reflections	36,503	
Resoltuion (Å)	35.86 – 2.88 (3.00 – 2.90)	
R_{merge}	0.18 (0.97)	
Mean I/σ(I)	10.8 (1.14)	
Completeness (%)	92.7 (76.5)	
Redundancy	4.2 (2.8)	
Refinement		
Resolution (Å)	35.86 – 2.90	
Number of reflections (test set)	35,504 (1,774)	
Rwork / Rfree	0.236 / 0.265	
Number of atoms	A	B
Protein	3,480	3,452
Ligand	34	34
Lipids and other	24	69
Mean Overall B value (Å^2)	A	B
protein	87	81
T4 lysozyme	82	75
Ligand	65	71
Lipids and other	106	80
R.m.s. deviations		
Bond lengths (Å)	0.005	
Bond angles (°)	0.83	
Ramanchandran plot statistics (%)*		
Favored regions	97.27	
Allowed regions	2.73	
Disallowed regions	0.0	

* As defined in MolProbity

Supplementary Table 2. Comparative pharmacology of WT hKOR and hKOR-T4L construct used for crystallization.

Agonist	WT hKOR Ki in nM expressed in HEK 293-T cells	hKOR (I135L) Ki in nM expressed in *Sf*9 cells	hKOR (I135L)-T4L Ki in nM expressed in *Sf*9 cells
U69593	39.8 (7.4±0.034)	91.8 (7±0.13)	65.76 (7.18±0.056)
Dynorphin A (1-17)	14.86 (7.8±0.2)	113.24 (6.9±0.22)	135.21 (6.87±0.107)
Bremazocine (–)	0.21 (9.7±0.054)	0.25 (9.6±0.036)	0.32 (9.49±0.069)
Cyclazocine (–)	0.95 (9.02±0.21)	2.95 (8.5±0.071)	4.54 (8.34±0.104)
β-endorphin	909.9 (6.04) ±0.31)	3069 (5.5±0.75)	1114.3 (5.95±0.443)

Data represent mean K_i (pK_i ± SD) for competition binding experiments using ^{3}H-diprenorphin as radioligand (0.2-0.5 nM final concentration). As can be seen, prototypical KOR agonists (U69593, bremazocine, cyclazocine) and β-endorphin display similar binding affinity for WT hKOR and hKOR-T4L constructs while the affinity for the endogenous agonist dynorphin (1-17) is attenuated, perhaps due to expression in a non-native environment, as the full-length receptor expressed in *Sf*9 cells also displayed lower affinity for dynorphin A (1-17).

Supplementary Table 3. Mutagenesis data for JDTic, nor-BNI and GNTI

KOR Mutant	Diprenorphine K_i, nM	JDTic K_i, nM	nor-BNI K_i, nM	GNTI K_i, nM
WT	0.77 (9.1 ± 0.1)	0.31 (9.5 ± 0.24)	0.67 (9.2 ± 0.12)	0.11 (9.95 ± 0.13)
hKOR (I135L)	1.2 (8.69)	0.27 (9.56 ± 0.1)	0.85 (9.07 ± 0.2)	ND
hKOR (I135L)-T4L	1.4 (8.74)	0.6 (9.2 ± 0.3)	2.3 (9.2 ± 0.3)	ND
H291F	0.91 (9.04 ± 0.03)	0.93 (9.03 ± 0.1)	0.8 (9.1 ± 0.31)	35.9 (7.45 ± 0.2)*
H291K	NSB	NSB	NSB	NSB
D138A	1.8 (8.76 ± 0.1)	26.9 (7.57 ± 0.09)*	3.87 (8.4 ± 0.13)*	2.8 (8.55 ± 0.11)*
I294S	1.7 (8.77 ± 0.1)	0.28 (9.55 ± 0.13)	30 (7.53 ± 0.2)*	29 (7.54 ± 0.1)*
E297A	0.9 (9.03 ± 0.04)	0.13 (9.9 ± 0.05)	7.8 (8.11 ± 0.24)*	22 (7.66 ± 0.13)*

***p<0.05 vs WT.** Data represent mean K_i in nM and, in parentheses, mean pK_i ± SD of parameter estimates for N=2-6 separate experiments. For each K_i determination 8-12 point competition binding experiments were performed with N=3-4 separate determinations at each point. ND=not done; NSB=no specific binding. Mutations were introduced into an N-terminal FLAG-tagged hKOR as previously described[1]. Transfections in HEK 293-T cells were performed as described by Jordan et al.[2]

Supplementary Table 4. Competitive binding data for salvinorin A at KOR mutants.

Residue[a]	KOR mutant	K_i (nM) ± SEM[b]	mut/wt K_i ratio[c]	Ref.
—	wt	31.6 ± 6.5	1	3
—	wt	17.5 ± 1.5	1	4
—	wt	23.5 ± 5.7	1	5
—	wt	33 ± 8	1	6
2.53	V108A	269 ± 25	11.4	5
2.53,2.63	V108A,V118K	>5000	>200	5
2.53	V108L	4.1 ± 0.8	0.2	5
2.55	T110S	28 ± 5.3	1.2	5
2.57	M112L	73.5 ± 20.8	3.1	5
2.60	Q115A	147 ± 47	8.4	4
2.60	Q115A	556 ± 231	17	6
2.63	V118K	846 ± 176	35.9	5
2.64	Y119A	342 ± 40	11	3
2.64	Y119A	67 ± 7.4	3.8	4
2.64	Y119F	233 ± 66	7	3
2.64	Y119F	17.7 ± 3.9	1	4
3.27	I133A	19.1 ± 4.6	0.8	5
3.29	I135L	99.1 ± 28.4	4.2	5
3.32	D138A	17.5 ± 4.4	1	4
3.33	Y139A	53.9 ± 13.9	2	3
3.33	Y139F	193 ± 38	6	3
3.33	Y139F	9.5 ± 2.8	0.54	4
ECL2	S211A	38 ± 5	1.2	6
ECL2	L212A	1.7 ± 1	0.05	6
ECL2	Q213A	40 ± 12	1.2	6
ECL2	F214A	1 ± 0.1	0.03	6
6.55	I294A	12 ± 6	0.4	6
6.58	E297A	19.5 ± 3.1	1.1	4
6.58	E297A	15 ± 3	0.5	6
7.35	Y312A	88.6 ± 10.9	3	3
7.35	Y312A	79 ± 28	4.5	4
7.35	Y312F	65.1 ± 11	2	3
7.35	Y312F	16 ± 3.8	0.91	4
7.36	Y313A	694 ± 106	22	3
7.36	Y313A	126 ± 48	7.2	4
7.36	Y313F	63.3 ± 15.2	2	3
7.36	Y313F	37 ± 3.7	2.1	4
7.43	Y320A	380 ± 103	12	3
7.43	Y320A	565 ± 49	32	4
7.43	Y320F	301 ± 75	10	3
7.43	Y320F	71 ± 15	4.1	4

[a]Ballesteros–Weinstein index. [b]Hot ligand = [^{3}H]diprenorphine. [c]Colors indicate magnitude of change: green, < 3×; yellow, 3–10×; red, ≥ 10×.

Supplementary Table 5. Interatomic distances (*d*) between heavy atoms of RB-64 and hKOR. Both adducts (+463 and +431) have essentially the same location and orientation. Colors indicate maximum magnitude of change observed for salvinorin A upon mutagenesis: green, < 3×; blue, 3–10×; red, ≥ 10×; black, not tested (see Supplementary Table 4). Corresponding mutagenesis references are given in parentheses.

	Interatomic Distance (Å)				
Ligand	***d* ≤ 3.0**	**3.0 < *d* ≤ 3.5**	**3.5 < *d* ≤ 4.0**	**4.0 < *d* ≤ 4.5**	**4.5 < *d* ≤ 5.0**
RB-64	T111$^{2.56}$ Y312$^{7.35}$ (ref [3,4]) Y313$^{7.36}$ (ref [3,4]) **C315$^{7.38}$**	W124^{ECL1} V134$^{3.28}$ D138$^{3.32}$ (ref [4]) I290$^{6.51}$ I316$^{7.39}$	V108$^{2.53}$ (ref [5]) Q115$^{2.60}$ (ref [4,6]) V118$^{2.63}$ (ref [5]) I137$^{3.31}$ C210^{ECL2} I294$^{6.55}$ (ref [6]) L309$^{7.32}$	L135$^{3.29}$ (ref [5]) Y320$^{7.43}$ (ref [3,4])	NONE

Supplementary Figures:

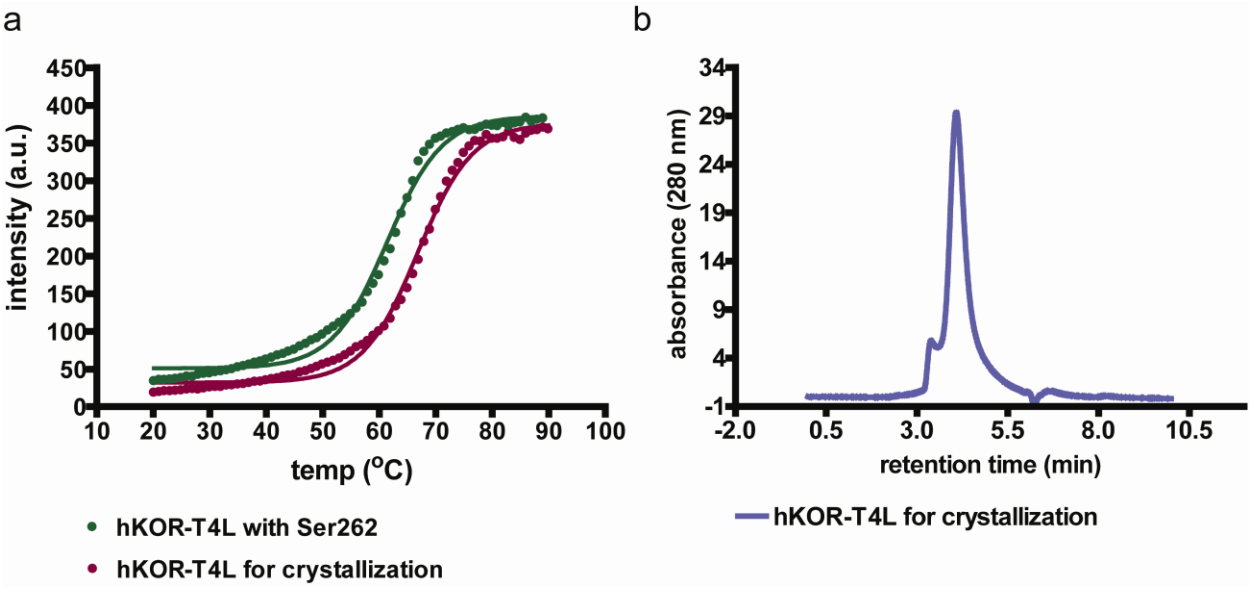

Supplementary Figure 1. Optimization of hKOR-T4L construct for crystallization. A. One residue of ICL3, Ser262, was deleted to enhance the thermal stability of the fusion protein. Thermal stability comparison between hKOR-T4L construct with Ser262 (Tm = 61 °C) and hKOR-T4L construct without Ser262 (Tm = 67 °C). The construct with Ser262 deleted was selected for structural study based on its higher thermal stability. Thermal stability assays were done as previously described.[7] **B.** Analytical size-exclusion chromotography (aSEC) of hKOR-T4L construct used in structural study showed a symmetrical peak, indicating the purified protein was monodisperse and homogenous. The protein monodispersity in detergent micelles system was achieved by N/C-terminal truncations (ΔGlu2-Ala42, ΔArg359-Val380).

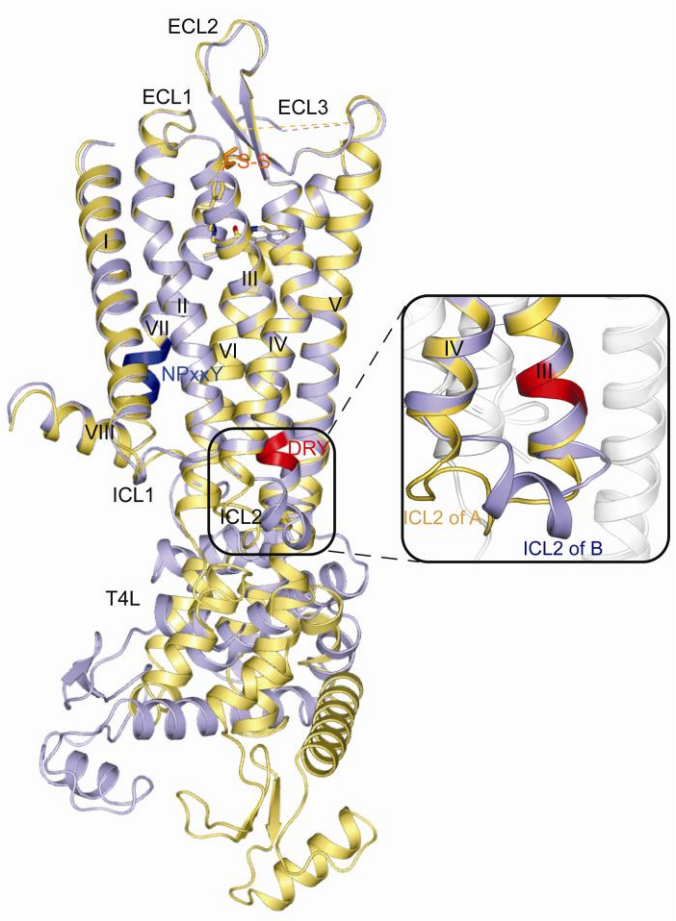

Supplementary Figure 2. Overall architecture of the hKOR-T4L-JDTic complex. Alignment of the A molecule and the B molecule through the receptor part. DRY motif is highlighted in red, NPxxY motif is highlighted in blue. One single point mutation in transmembrane helix III (Ile135$^{3.29}$Leu; superscripts indicate residue numbers as per the Ballesteros-Weinstein nomenclature[8]) was implemented as it was reported to increase KOR expression[5]. Residues constituting the 7-TM α helices are Ala57$^{1.30}$ – Tyr87$^{1.60}$ (helix I; superscripts indicate residue numbers as per the Ballesteros –Weinstein (Ba-We) nomenclature; Ala93$^{2.38}$ – Met121$^{2.66}$ (helix II); Asp128$^{3.22}$ – Cys161$^{3.55}$ (helix III); Arg170$^{4.37}$ – Leu196$^{4.63}$ (helix IV); Tyr219$^{5.31}$ – Arg257$^{5.69}$ (helix V); Arg267$^{6.28}$ – Leu299$^{6.60}$ (helix VI); Leu309$^{7.32}$ – Leu333$^{7.56}$ (helix VII). Helix VIII, a small membrane-parallel helix of hKOR, comprised of residues Glu335 – Phe344. Residues defining intracellular and extracellular loops (ICLs and ECLs) are Thr88 – Thr92 (ICL1); Asn122 – Gly127 (ECL1); His162 – Phe169 (ICL2); Gly197 – Asp218 (ECL2); Leu258 – Asp266 (ICL3); Gly300 – Ala310 (ECL3). The difference of ICL2 secondary structure between molecules A and B is highlighted by insert. The graphics were created by PyMOL.

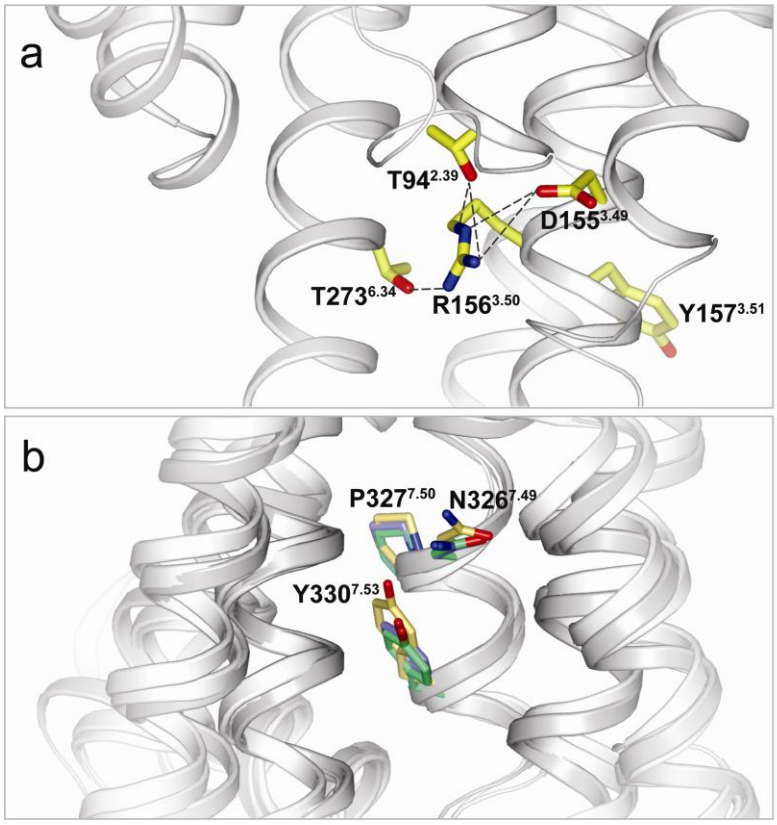

Supplementary Figure 3. The DRY and NPxxY motifs of hKOR. (**A**) Arg156$^{3.50}$ from the DRY motif forms a hydrogen bond to the side chain of Thr273$^{6.34}$ at the cytoplasmic end of helix VI (distance of 3.2 Å), which is proposed to stabilize the inactive state of hKOR. The guanidinium group of Arg156$^{3.50}$ is poised for its interaction with helix VI, through stabilizing H-bonding interactions between Asp155$^{3.49}$ of the DRY motif and Thr94$^{2.39}$ at the cytoplasmic end of helix II (distances between Thr94 and Arg156 are 3.8 and 4.0 Å, respectively; distances between Asp155 and Arg156 are 3.4 and 3.6 Å, respectively). (**B**). Comparison of hKOR (yellow) and inactive β_2AR (blue, PDB ID: 2RH1) and A_{2A}AR (green, PDB ID: 3EML) structures shows a similar conformation and position of the NPxxY motif among these three structures. Parts of helix III in all three receptors are removed for clarity. Helices of hKOR are colored gray, and helices of β_2AR and A_{2A}AR are colored white. The graphics were created by PyMOL.

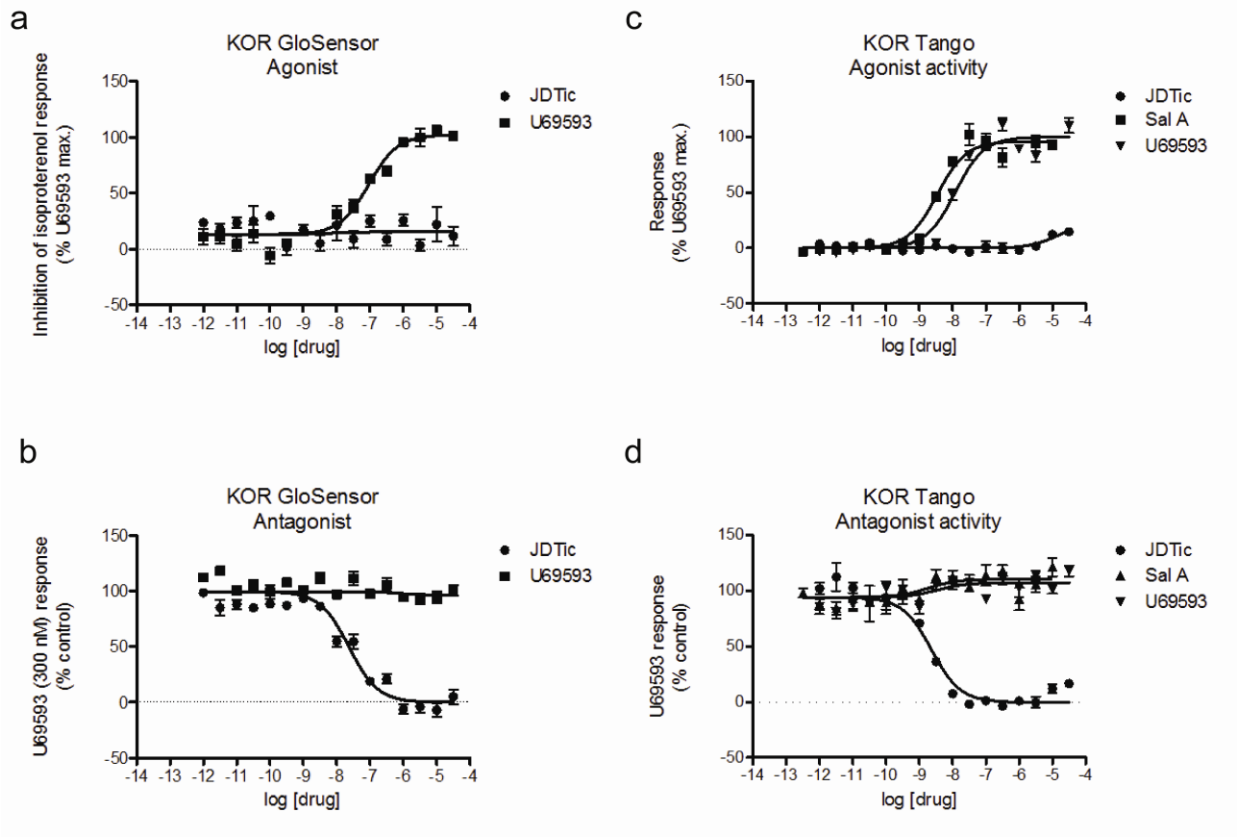

Supplementary Figure 4. JDTic is an antagonist for KOR-mediated cAMP production and KOR-mediated arrestin activity. There is some controversy regarding the functional properties of JDTic – in particular whether JDTic induces a long-lasting activation of KOR-mediated phosphorylation of c-Jun N-terminal kinase[9], or whether JDTic functions as a KOR antagonist. As JDTic has not previously been rigorously studied in canonical and non-canonical signaling assays, we evaluated JDTic's ability to modulate G_i-mediated and β-arrestin-mediated signaling in transfected HEK 293-T cells. (**A**) and (**B**) Shown is a representative experiment where JDTic was evaluated for agonist and antagonist activity for KOR-mediated inhibition of cAMP response using a cAMP biosensor (for details see ref[10]). The EC_{50} for the canonical KOR agonist U69593 was 91 nM and JDTic had a K_i value of 22 nM. (**C**) and (**D**) JDTic is an antagonist for KOR-mediated arrestin activity. Shown in (**C**) are representative concentration-response curves for the effects of representative KOR agonists (U69593, salvinorin A) and JDTic on KOR-mediated arrestin activity. As can be seen, JDTic is devoid of agonist activity while (**D**) shows that JDTic potently inhibits U69593-stimulated arrestin activity as measured by the Tango assay (see ref [11] for details). In this assay JDTic had a K_i of 0.09 nM. These results are most consistent with the structural data indicating that JDTic stabilizes an inactive conformation of KOR.

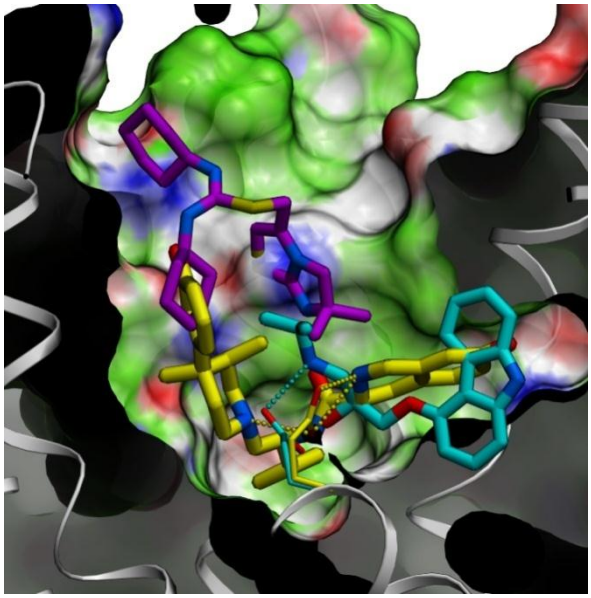

Supplementary Figure 5. Positions of ligands in superimposed crystal structures of hKOR, β_2AR and CXCR4. Sliced hKOR binding pocket is shown by skin colored by binding properties (green: hydrophobic, blue: H-bond donor, red: H-bond acceptor). JDTic ligand (shown with yellow carbons) position is compared to positions of carazolol in β_2AR (cyan carbons; from PDB ID 2RH1) and IT1t in CXCR4 (magenta carbons; from PDB ID 3ODU). Note the similarity in JDTic and carazolol binding, both are anchored by salt bridge interactions with acidic Asp side chain in position 3.32. In contrast, the shallow binding pocket of CXCR4 (not shown) dictates a much higher position of IT1t close to the extracellular loops. The graphics were prepared using ICM molecular modeling package (Molsoft LLC).

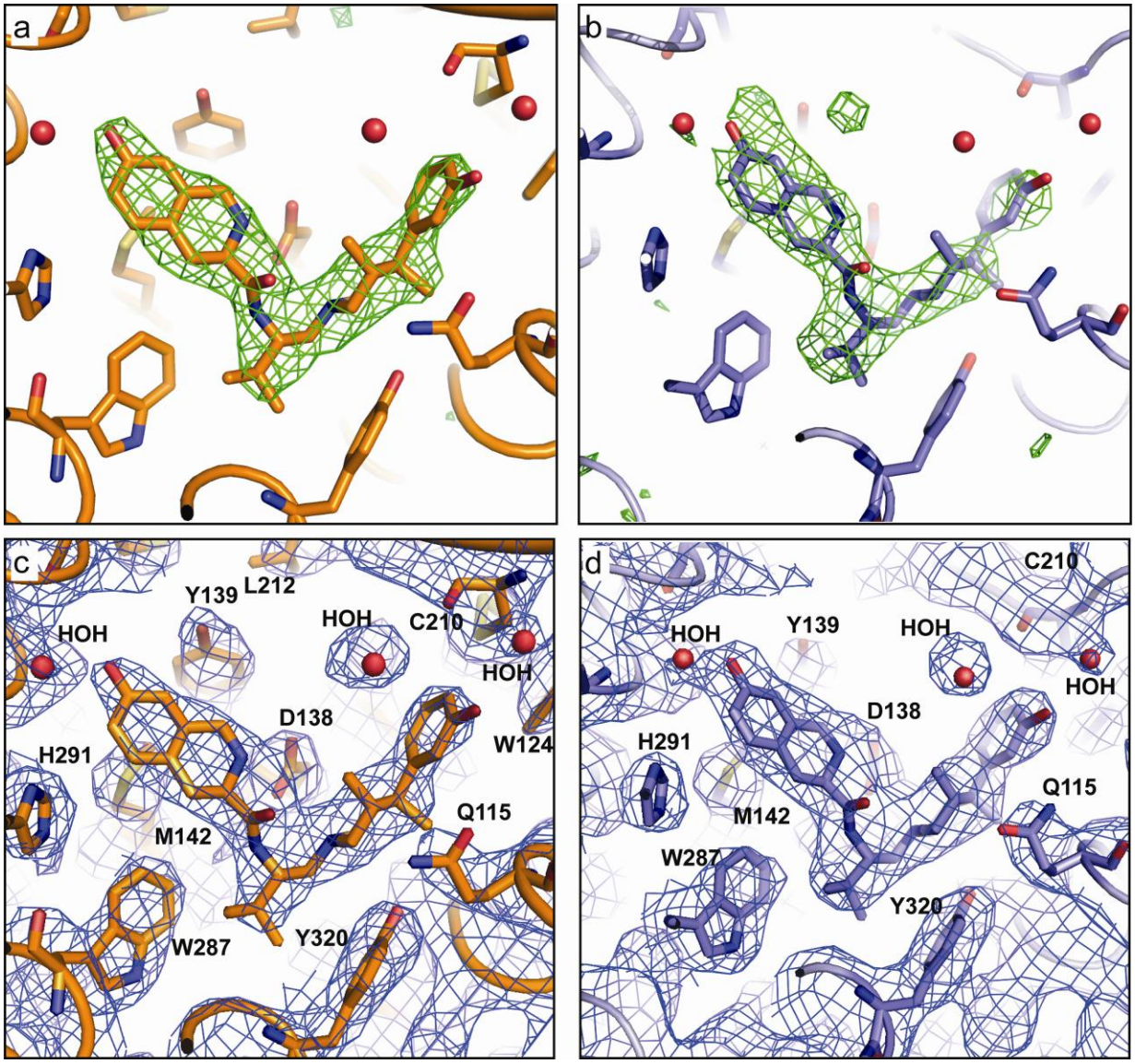

Supplementary Figure 6. Examples of the electron density maps calculated from the refined model for hKOR-JDTic complex. $|F_o|-|F_c|$ omit maps (green mesh) of the ligand JDTic in (**A**) A molecule (**B**) B molecule within one asymmetric unit, contoured at 3.0σ (0.15 e/Å). $2|F_o|-|F_c|$ maps (blue mesh) for the ligand binding pockets of (**C**) A molecule and (**D**) B molecule, contoured at 1.0σ (0.10 e/ Å). Water molecules are shown in red sphere representation. The graphics were created by PyMOL.

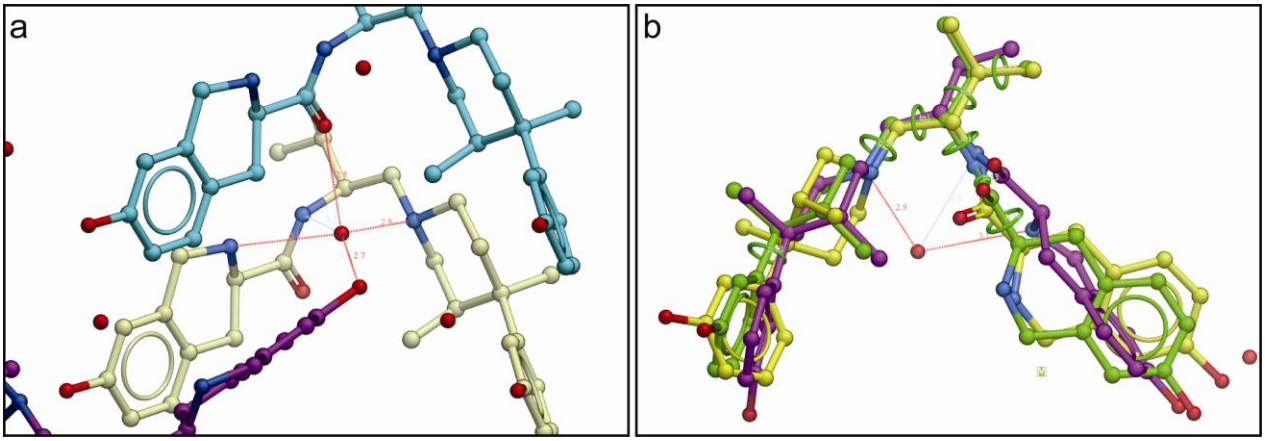

Supplementary Figure 7. Crystal Structure of JDTic. (**A**) A crystallographic water molecule coordinates with amino groups of one of the JDTic molecules (shown with white carbons) and hydrogen bonds to two other JDTic molecules in the crystal lattice (shown by cyan and magenta) (**B**) Comparison of the three conformations of JDTic: found in hKOR-JDTic crystal structure (yellow), found by energy optimization of JDTic (green) and found in free JDTic crystals (magenta). The graphics were prepared using ICM molecular modeling package (Molsoft LLC).

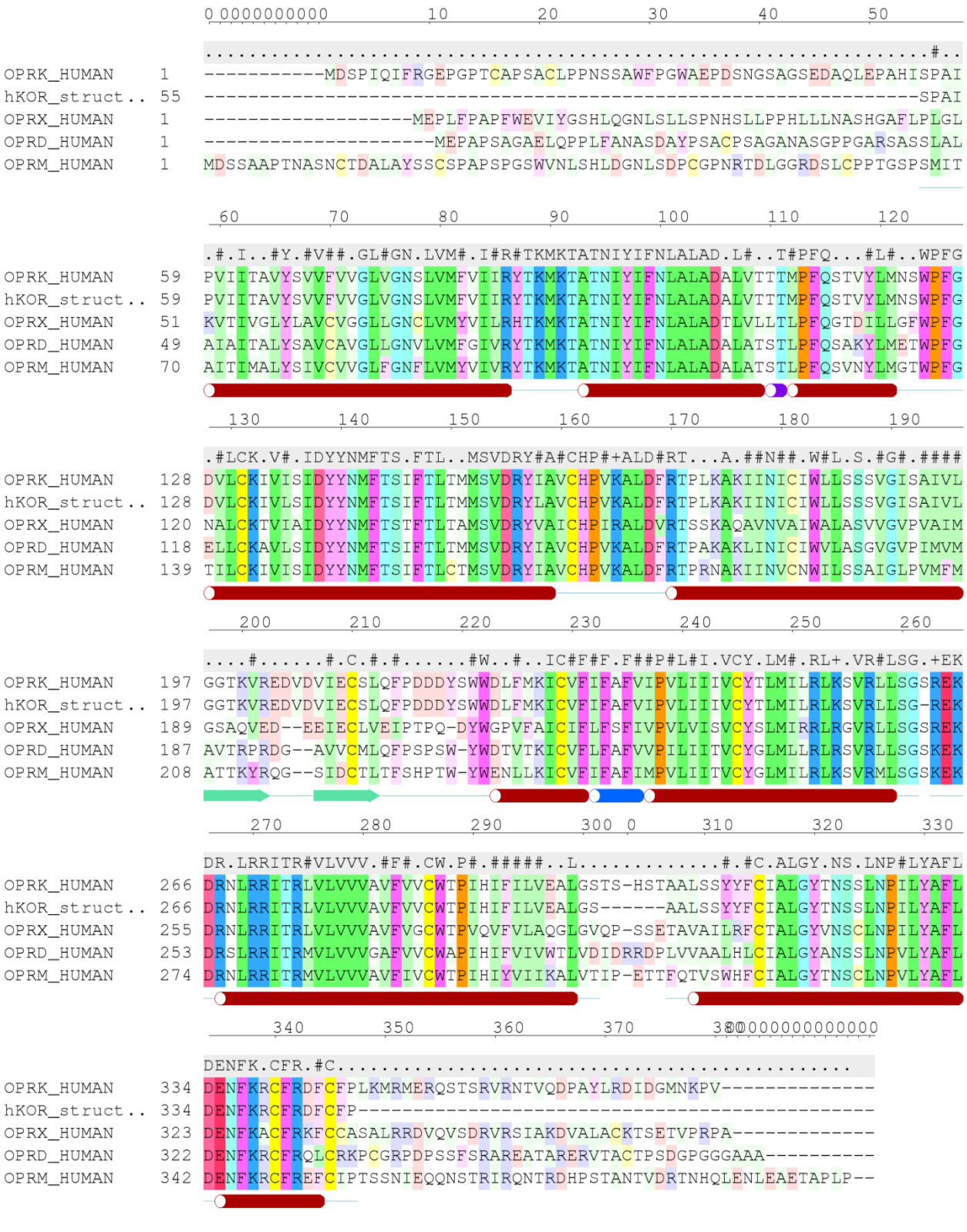
OPRK_HUMAN
hKOR_struct..
OPRX_HUMAN
OPRD_HUMAN
OPRM_HUMAN

Supplementary Figure 8. **Sequence alignment of hKOR with other OR subtypes.** Amino acid sequences of hKOR (OPRK), hMOR (OPRM), hDOR (OPRD) and the nociceptin/orphanin FQ peptide receptor (OPRX) are shown. The second line shows the structurally resolved part of the hKOR sequence (hKOR_struct), while the other sequences are obtained from Uniprot. Secondary structure of hKOR is displayed below alignment (red: α-helix, blue: π-helix, green: β-strands). Uncolored residues show lack of conservation, while coloring highlights conserved amino acids with specific functional properties (green: hydrophobic, blue: basic, red: acidic, magenta: aromatic, cyan: small polar, orange: proline, yellow: cysteine). N and C-termini and ECL3 loop do not have significant sequence homology. The graphics were prepared using ICM molecular modeling package (Molsoft LLC).

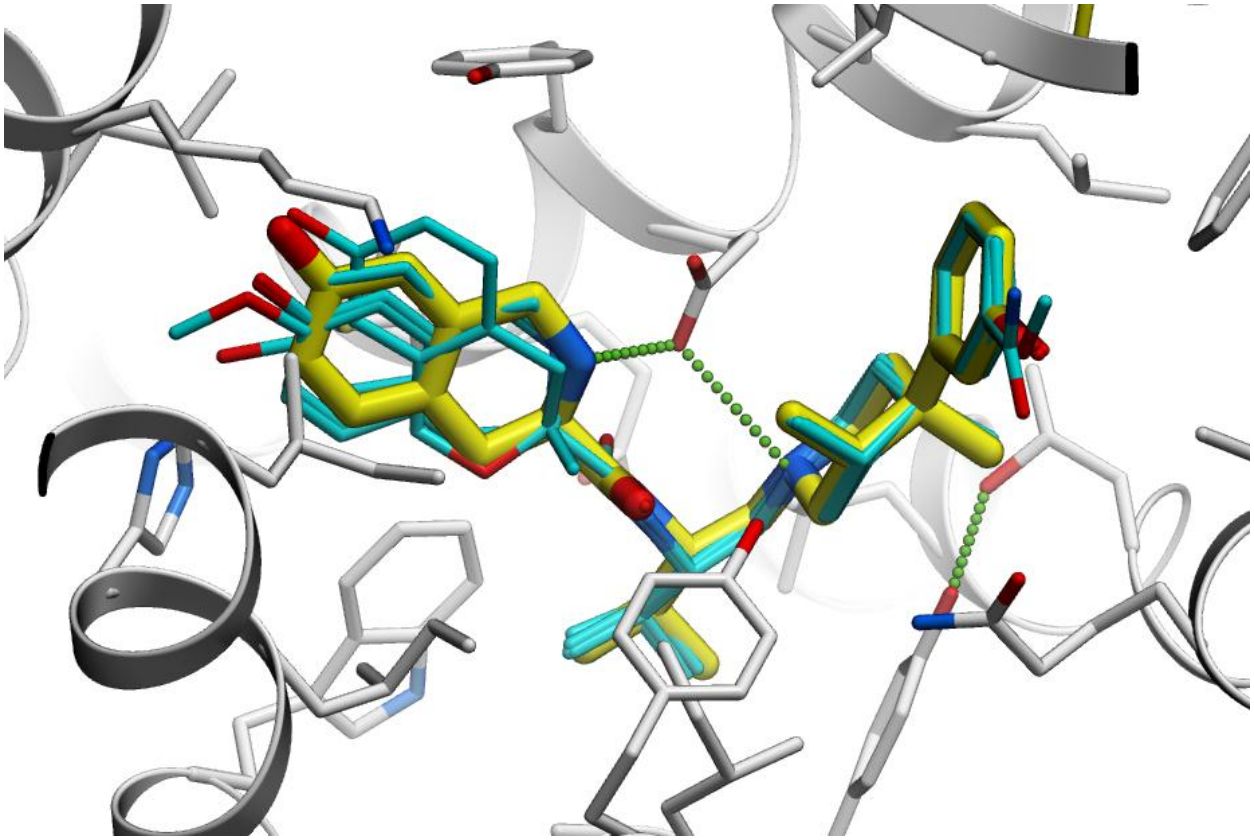

Supplementary Figure 9. Comparison of JDTic pose in the crystal structure (yellow carbons) with results of docking of high-affinity JDTic analogues (cyan carbons). Overlapping poses of docked compounds **2** (from ref [12]), **8b**, **8d**, **8e** (from ref [13]), and **8a** (from ref [14]) are shown. The binding poses of analogs suggest very high conservation of the trans-(3R,4R)- dimethyl-4-(3-hydroxyphenyl)piperidine scaffold binding, while optimal fit of the variable bicyclic moiety involves some modifications in its position. Docking of JDTic analogs was performed using energy-based flexible docking in ICM molecular modeling package (Molsoft LLC) as described in Methods section. The graphics were prepared using the ICM molecular modeling package (Molsoft LLC).

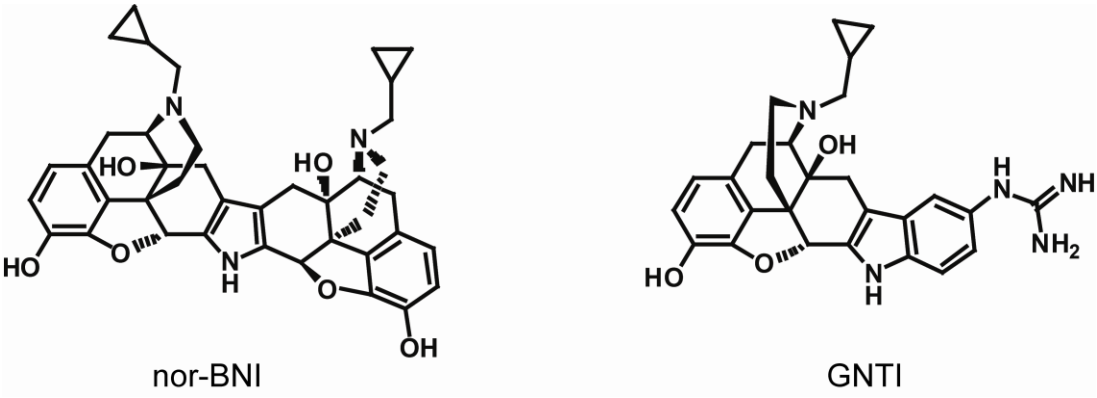

Supplementary Figure 10. Chemical structures of KOR selective antagonists nor-BNI and GNTI.

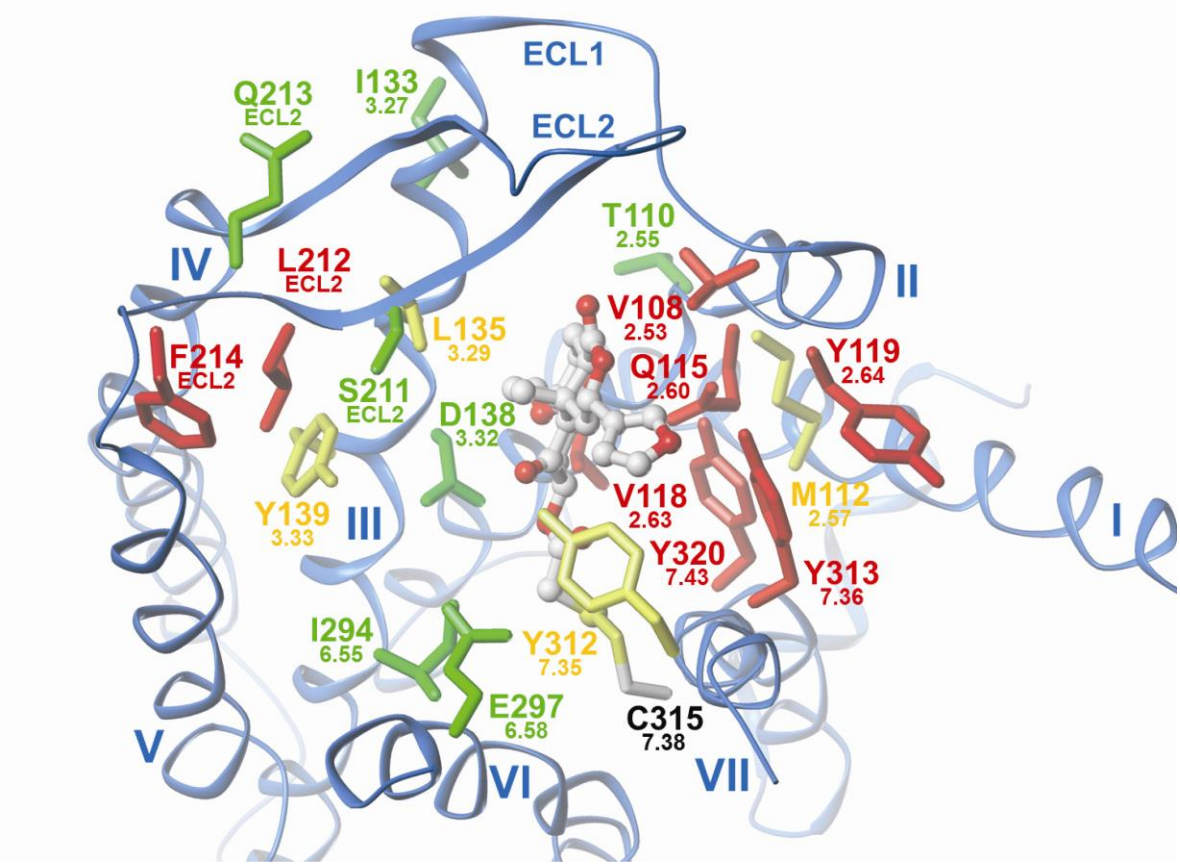

Supplementary Figure 11. Docked structure of RB-64 (+463 adduct) illustrating its interaction and/or close association with hKOR residues V108, Q115, V118, Y119, Y313 and Y320 that cause a substantial (≥ 10×) decrease in the affinity of SalA for hKOR upon mutation. Five of the six aforementioned residues are within 4.5 Å of RB-64. Two residues on ECL2 (L212 and F214), distant from the previously mentioned group, substantially *increase* the affinity of SalA for hKOR when mutated to alanine, indicating an indirect effect, as opposed to direct interaction with the ligand. hKOR residues are color-coded as in Supplementary Table 4 (green, < 3×; yellow, 3–10×; red, ≥ 10×).

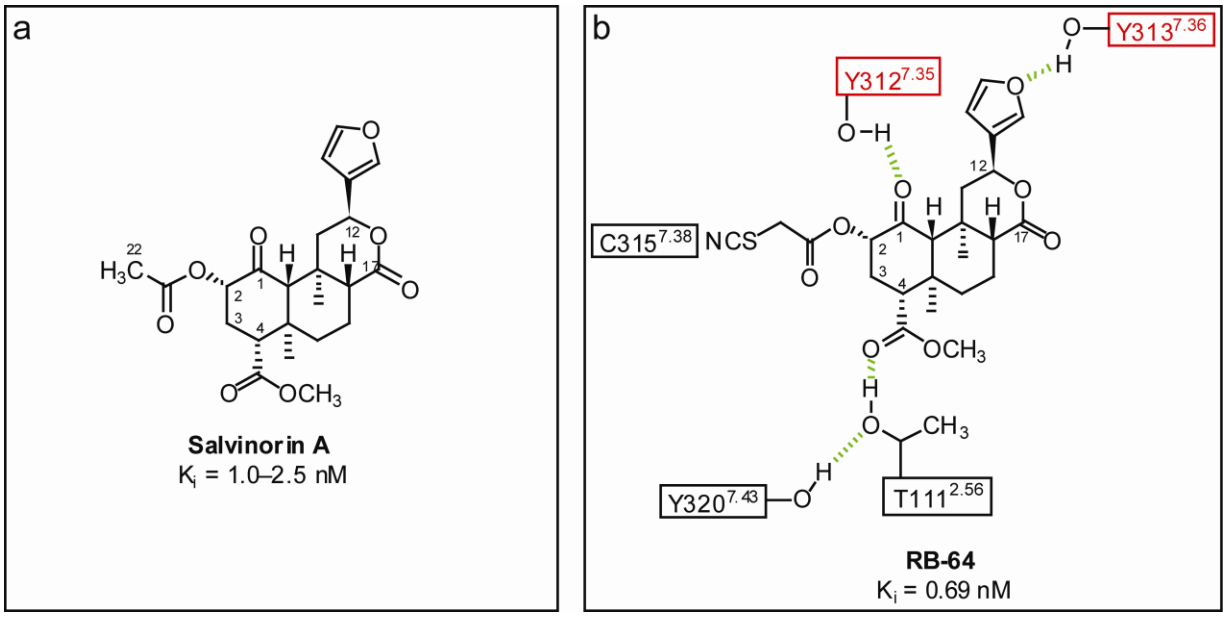

Supplementary Figure 12. Schematic diagrams of (**A**) SalA and (**B**) RB-64–hKOR polar interactions. Residues that are unique to hKOR are shown in red. Hydrogen bonds are shown in green.

Literature Cited

1 Yan, F. *et al.* Structure-based design, synthesis, and biochemical and pharmacological characterization of novel salvinorin A analogues as active state probes of the kappa-opioid receptor. *Biochemistry* **48**, 6898-6908, (2009).

2 Jordan, M., Schallhorn, A. & Wurm, F. M. Transfecting mammalian cells: optimization of critical parameters affecting calcium-phosphate precipitate formation. *Nucleic Acids Res* **24**, 596-601, (1996).

3 Yan, F. *et al.* Identification of the molecular mechanisms by which the diterpenoid salvinorin A binds to kappa-opioid receptors. *Biochemistry* **44**, 8643-8651, (2005).

4 Kane, B. E., Nieto, M. J., McCurdy, C. R. & Ferguson, D. M. A unique binding epitope for salvinorin A, a non-nitrogenous kappa opioid receptor agonist. *FEBS J* **273**, 1966-1974, (2006).

5 Vortherms, T. A., Mosier, P. D., Westkaemper, R. B. & Roth, B. L. Differential helical orientations among related G protein-coupled receptors provide a novel mechanism for selectivity. Studies with salvinorin A and the kappa-opioid receptor. *J Biol Chem* **282**, 3146-3156, (2007).

6 Yan, F., Mosier, P. D., Westkaemper, R. B. & Roth, B. L. Galpha-subunits differentially alter the conformation and agonist affinity of kappa-opioid receptors. *Biochemistry* **47**, 1567-1578, (2008).

7 Alexandrov, A. I., Mileni, M., Chien, E. Y., Hanson, M. A. & Stevens, R. C. Microscale fluorescent thermal stability assay for membrane proteins. *Structure* **16**, 351-359, (2008).

8 Ballesteros, J. A. & Weinstein, H. Integrated methods for the construction of three-dimensional models and computational probing of structure-function relations in G protein-coupled receptors. *Methods Neurosci* **25**, 366-428, (1995).

9 Bruchas, M. R. *et al.* Long-acting kappa opioid antagonists disrupt receptor signaling and produce noncompetitive effects by activating c-Jun N-terminal kinase. *J Biol Chem* **282**, 29803-29811, (2007).

10 Kimple, A. J. *et al.* Structural determinants of G-protein alpha subunit selectivity by regulator of G-protein signaling 2 (RGS2). *J Biol Chem* **284**, 19402-19411, (2009).

11 Allen, J. A. *et al.* Discovery of beta-Arrestin-Biased Dopamine D2 Ligands for Probing Signal Transduction Pathways Essential for Antipsychotic Efficacy. *Proc Natl Acad Sci U S A* **108**, 18488-18493, (2011).

12 Cai, T. B. *et al.* Synthesis and in vitro opioid receptor functional antagonism of analogues of the selective kappa opioid receptor antagonist (3R)-7-hydroxy-N-((1S)-1-{[(3R,4R)-4-(3-hydroxyphenyl)-3,4-dimethyl-1-pipe ridinyl]methyl}-2-methylpropyl)-1,2,3,4-tetrahydro-3-isoquinolinecarboxami de (JDTic). *J Med Chem* **51**, 1849-1860, (2008).

13 Cueva, J. P. *et al.* Synthesis and in vitro opioid receptor functional antagonism of methyl-substituted analogues of (3R)-7-hydroxy-N-[(1S)-1-{[(3R,4R)-4-(3-hydroxyphenyl)-3,4-dimethyl-1-pipe ridinyl]methyl}-2-methylpropyl]-1,2,3,4-tetrahydro-3-isoquinolinecarboxami de (JDTic). *J Med Chem* **52**, 7463-7472, (2009).

14 Runyon, S. P. *et al.* Analogues of (3R)-7-hydroxy-N-[(1S)-1-{[(3R,4R)-4-(3-hydroxyphenyl)-3,4-dimethyl-1-pipe ridinyl]methyl}-2-methylpropyl)-1,2,3,4-tetrahydro-3-isoquinolinecarboxami de (JDTic). Synthesis and in vitro and in vivo opioid receptor antagonist activity. *J Med Chem* **53**, 5290-5301, (2010).